Direct Modeling of X-Ray Diffraction Pattern from Skeletal Muscle in Rigor

Natalia A. Koubassova and A. K. Tsaturyan
Institute of Mechanics, Lomonosov Moscow State University, Vorobjovy Gory, Moscow 119992, Russia

ABSTRACT Available high-resolution structures of F-actin, myosin subfragment 1 (S1), and their complex, actin-S1, were used to calculate a 2D x-ray diffraction pattern from skeletal muscle in rigor. Actin sites occupied by myosin heads were chosen using a "principle of minimal elastic distortion energy" so that the 3D actin labeling pattern in the A-band of a sarcomere was determined by a single parameter. Computer calculations demonstrate that the total off-meridional intensity of a layer line does not depend on disorder of the filament lattice. The intensity of the first actin layer A1 line is independent of tilting of the "lever arm" region of the myosin heads. Myosin-based modulation of actin labeling pattern leads not only to the appearance of the myosin and "beating" actin-myosin layer lines in rigor diffraction patterns, but also to changes in the intensities of some actin layer lines compared to random labeling. Results of the modeling were compared to experimental data obtained from small bundles of rabbit muscle fibers. A good fit of the data was obtained without recourse to global parameter search. The approach developed here provides a background for quantitative interpretation of the x-ray diffraction data from contracting muscle and understanding structural changes underlying muscle contraction.

INTRODUCTION

X-ray diffraction was the first source of information about muscle structure at the molecular level (Huxley, 1996). During the last two decades, this method was significantly improved by using bright synchrotron radiation sources and modern 2D detectors (Harford and Squire, 1997), so that its spatial (Huxley et al., 1994; Wakabayashi et al., 1994; Linari et al., 2000) and time (Dobbie et al., 1998) resolutions are now significantly higher than provided by other methods used for structural studies of muscle. Quantitative interpretation of the diffraction data is not straightforward due to the absence of phase information, so the Fourier synthesis cannot be exploited. Direct modeling of 2D x-ray diffraction data using available information about the structure of the myosin rod and heads was successfully used to study packing of the myosin heads in relaxed muscles of different specimens (Malinchik and Lednev, 1992; Malinchik et al., 1997; Hudson et al., 1997). Positions of the heads on the myosin backbone were determined using global parameter search.

Quantitative interpretation of the diffraction data from contracting or rigor muscle was limited by simple models describing only one or a very few x-ray reflections. The main difficulty in direct modeling of the whole 2D x-ray diffraction pattern from muscle in the states where myosin heads interact with actin is the complexity of the 3D structure of the actin-myosin lattice. The number of parameters needed to describe the position of each myosin head is very high in this case, and the model becomes too complex to be practical. Instead, one can use a parametrization procedure that significantly reduces the number of parameters.

In rigor (i.e., in the absence of nucleotide) all myosin heads tightly and stereospecifically bind actin (Cooke and Franks, 1980; Lovell et al., 1981; Cooke et al., 1984). The configuration of the actin-myosin complex in rigor is believed to be the same or very similar to the structure of the actin-S1 complex in solution. Structurally, rigor is a well-defined state in which muscles or single muscle fibers produce a rich set of layer lines on the x-ray diffraction pattern (Huxley and Brown, 1967; Bershitsky et al., 1996; Xu et al., 1997; Takezawa et al., 1999). These make rigor a convenient state for direct modeling of the x-ray diffraction pattern. A model of the rigor state can be considered as the first step toward the more complex problem of giving a quantitative description of the actin-myosin structure in contracting muscle where the number of myosin heads attached to actin and their orientation with respect to the thin filaments are less known.

To set the actin labeling pattern in rigor insect flight muscle, Holmes et al. (1980) introduced a one-dimensional binding probability function depending on only a few parameters. Squire and Harford (1988) tested several algorithms to produce an actin labeling pattern in rigor. Using only the locations of the actin sites labeled by the myosin heads, they calculated the intensities of the layer lines and found good agreement between the computed and experimental diffraction patterns for a model in which the azimuthal movement of the heads away from their position on the three-strand helix of the myosin rod is within the range of $-60°$ to $+60°$.

At present, high-resolution structures of F-actin (Holmes et al., 1990; Lorenz et al., 1993), of the myosin head or S1 (Rayment et al., 1993a), and of the actin-S1 complex (Rayment et al., 1993b; Mendelson and Morris, 1997; Holmes et al., 2002) are available. We used these data for a more

Submitted December 6, 2001, and accepted for publication April 2, 2002.
Address reprint requests to Dr. A. K. Tsaturyan, Institute of Mechanics, Lomonosov Moscow State University, Vorobjovy Gory, Moscow 119992, Russia. Tel.: 7-095-939-12-52; Fax: 7-095-939-01-65; E-mail: tsat@imec.msu.ru.
© 2002 by the Biophysical Society
0006-3495/02/08/1082/16 $2.00

precise determination of the actin labeling pattern and for quantitative modeling of the x-ray diffraction pattern. In our model the parametrization of the actin labeling was achieved with a physically plausible principle of "minimal elastic distortion energy." Axial and radial disorder of the actin-myosin lattice was also taken into account.

Our aim was not only to obtain the best fit to a particular experimental diffraction pattern. Rather, it was to develop a quantitative understanding of how the structure of the actin-S1 complex and the parameters that control the binding pattern and disorder of the filament lattice affect observed diffraction pattern. Some results of the modeling were briefly described earlier (Koubassova and Tsaturyan, 1999).

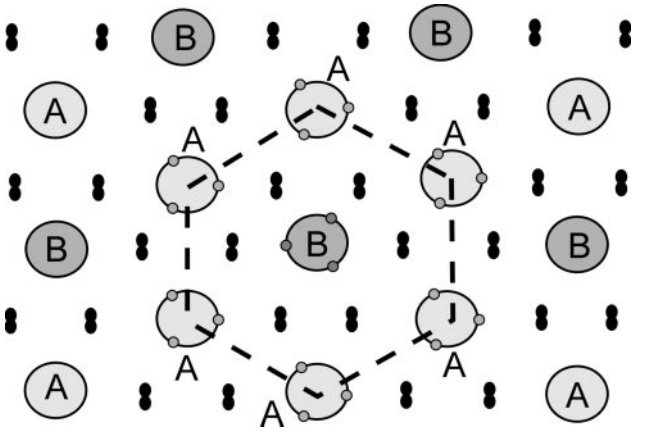

FIGURE 1 Scheme of the super-lattice structure of the overlap zone in skeletal muscle. A section perpendicular to the filament axis is shown. The origins, i.e., the positions of the S1-S2 junctions, of the myosin heads on the backbone are represented by circles. Myosin filaments with two different orientations are marked by letters *A* and *B*. All actin filaments (shown by two dark circles) are supposed to have the same orientation. The dashed hexagon shows a super-lattice unit cell.

MATERIALS AND METHODS

Experimental x-ray diffraction pattern

The intensity distributions along the layer lines calculated from the model were compared with experimental data obtained in collaboration with S. Y. Bershitsky (Institute of Physiology, Ural Branch of the Russian Academy of Sciences, Yekaterinburg, Russia) and M. A. Ferenczi (National Institute for Medical Research, London) on beam line 16.1 of the Synchrotron Radiation Source at Daresbury Laboratory (Cheshire, UK) using a new RAPID 2D multiwire detector (Lewis et al., 1997). The detector operated at the resolution of 512 × 512 pixels with the sample-to-detector distance of 3.25 m. The experimental setup was described by Bershitsky et al. (1996, 1997). Rabbit muscle fibers from *m. psoas* were permeabilized as described by Thirlwell et al. (1994). Small bundles of permeabilized rabbit muscle fibers were put into rigor at a sarcomere length of 2.4 μm in the presence of BDM as described by Bershitsky et al. (1996) to preserve sarcomere structure. Then BDM was washed out with a rigor solution containing 100 mM TES, 2 mM Mg^{2+}, 5 EGTA, and 10 mM glutathione; the ionic strength of 150 mM was adjusted with potassium propionate (all chemicals from Sigma, St. Louis, MO), pH 7.1 at 20°C. Immediately before collection of the diffraction data, the chamber containing rigor solution was removed and the bundle was suspended in a water-saturated atmosphere at 6°C for 10 s when the x-ray shutter was opened. The pattern used for comparison with the model was collected from a bundle of seven muscle fibers with total x-ray exposure of 200 s.

The diffraction pattern was corrected for the detector response and camera background scattering, and averaged as described by Bershitsky et al. (1996). Radial distribution of the x-ray intensity along the layer lines was obtained as follows. The off-meridional part of the pattern was integrated along the equator and plotted against the meridional spacing to define the position and width of each layer line. Then a wide slice parallel to the equator and covering the meridional position of a layer was cut. Two-pixel-wide slices on both sides beyond the layer line were cut to obtain the background. Assuming linear variation in the background scatter over small distances, the radial distribution of the x-ray intensity along the layer lines was obtained by subtracting the intensities of the narrow slices (scaled for their width) from the intensity of the wide one at each radial position. To decrease noise, data points for the background slices were smoothed using spline functions. Also, the wide slices for all layer lines, except the most sampled first actin layer line, A1, and third myosin layer line, M3, were averaged over five neighbor pixels in the radial direction.

Unit cell

In some fish muscles where all myosin filaments have the same orientation (Squire and Harford, 1988) the actin-myosin lattice is simple and the unit cell contains one myosin and two actin filaments. In skeletal muscles of higher vertebrates myosin filaments can have one of two different orientations (Luther and Squire, 1980; Squire and Harford, 1988), and the actin and myosin filaments form an irregular super-lattice. We modeled this irregular super-lattice by a regular hexagonal lattice with a unit cell containing six actin and three myosin filaments in which the central myosin filament and its neighbors have different orientations (Fig. 1). The diamond unit cell that corresponds to this hexagonal cell has a side of $\sqrt{3}a$, where a is the distance between the centers of neighboring myosin filaments or the side of a simple lattice unit cell (Squire and Harford, 1988; Hudson et al., 1997).

The actin filament was considered as a 13/6 left-handed helix (Holmes et al., 1990). An axial distance of 2.75 nm between subsequent actin monomers in a thin filament was used in the model (experimental value is 2.73 nm; Huxley and Brown, 1967; Huxley et al., 1994), so that the pitch of the actin helix was 35.75 nm = 13 × 2.75 nm. The pitch of the right-handed three-strand myosin helix was taken as 42.9 nm or 3 × 14.3 nm, so the true axial repeat of the actin-myosin lattice (axial size of the unit cell) was in the model 214.5 nm = 6 × 35.75 nm = 5 × 42.9 nm, i.e., equal to six pitches of the actin helix or five pitches of the myosin helix. Experimental values for pitches of the actin and myosin helices for muscle in rigor are 0.7% higher than those used here: 36–37 nm for the first actin layer line (Huxley and Brown, 1967; Yagi, 1991; Kraft et al., 1998) and ≈43.2 = 3 × 14.4 nm for the first myosin layer line (Huxley and Brown, 1967; Xu et al., 1997). We also supposed that all actin filaments have the same azimuthal orientation defined by their fixation in the Z-line (Squire and Harford, 1988). The radius of the thick filaments was assumed to be 7.5 nm and the distance between the centers of neighbor myosin filaments a was 45.5 nm, so a super-lattice unit cell contained three myosin filaments, six actin filaments, 270 = 3 × 90 myosin heads, and 468 = 6 × 78 actin monomers.

Actin labeling pattern: principle of minimal elastic distortion energy

We assumed that in rigor all myosin heads are bound to actin (Lovell et al., 1981; Cooke et al., 1984) and that their catalytic domains have the same orientation with respect to actin as that found in isolated actin-S1 complexes (Rayment et al., 1993b; Mendelson and Morris, 1997; Holmes et al., 2002). To bind an actin site, a myosin head has to pull its "tail" (i.e.,

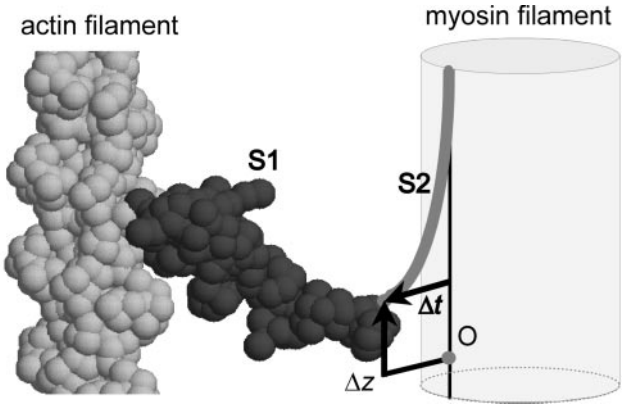

FIGURE 2 Scheme illustrating the principle of minimal elastic distortion energy. A myosin head, S1, is bound to an actin monomer on a thin filament. This binding is accompanied by bending of the tail domain of the myosin molecule, S2, and its detachment from the backbone of the myosin filament. Besides, to match the axial position of the actin monomer the light chain or the "neck" domain of S1 has to bend in a plane parallel to the fiber axis. Transversal, Δt, and axial, Δz, components of the displacement of the S1-S2 junction from its origin (○) on the backbone of the thick filament are associated with two components of elastic force, $k_t\Delta t$, and $k_z\Delta z$, where k_z and k_t are the bending stiffness of the S1 neck and S2, respectively.

subfragment 2, or S2) out of the myosin rod and bend it (Fig. 2). The detachment and bending of S2 is determined by its adhesion to the myosin rod and bending elasticity of S2 (Stewart et al., 1987). The binding is also accompanied by an axial displacement of the actin-binding region of the head from its equilibrium position. This displacement is most probably provided by bending of the light chain domain or "neck" region of S1 (Dobbie et al., 1998, Fig. 2). The total elastic energy, E, associated with binding of the head to actin can be expressed as $E = 0.5 \cdot (k_t(\Delta t)^2 + k_z(\Delta z)^2)$, where k_t and k_z are transversal and axial stiffness of a cross-bridge, i.e., bending stiffness of S2 and the S1 neck, respectively; Δt and Δz are, respectively, transversal and axial displacements of the S1-S2 junction from its "origin" on the surface of the myosin rod. The transversal displacement is a combination of radial and azimuthal movements. The "principle of minimal elastic distortion energy" means that a myosin head is always bound to the actin site that requires minimum elastic energy, E. Although the head can bind different actin sites, it spends most of the time being attached to the "most favorable" site.

Each molecule of skeletal muscle myosin II has two heads. Two different assumptions concerning their binding to actin were tested. In the first hypothesis ("forced pair" case), it was assumed that the two heads bind two adjacent actin sites on the same thin filament (Squire and Harford, 1988). These two sites are shifted axially by 5.5 nm and azimuthally by $2\pi/13$. In the second hypothesis ("free choice" case), the two heads were allowed to bind actin sites on different thin filaments if the binding of the second head to another thin filament results in less elastic distortion energy E. For each of the two hypotheses the pattern of actin labeling by bound myosin heads depends on a stiffness ratio, $e = k_t/k_z$, and on axial shift between the actin and myosin filaments, z_0, which in turn depends on the sarcomere length.

An algorithm of selection of actin monomers according to the principle of minimal elastic energy was as follows. On the first stage, two actin monomers that provide minimal elastic energy E were found for two heads of each myosin molecule in a super-lattice unit cell. In the case of "forced pairs" these actin sites were necessarily adjacent monomers on one filament. If two or more myosin heads "collide" with each other, preferring to bind the same actin monomer, new actin binding sites were chosen for each conflicting head (and for its "partner" in the "forced pairs" case) until all "conflicts" were resolved and the minimum possible sum of the elastic energies of the heads was achieved.

Sphere models of F-actin and myosin head

The electron densities of an actin monomer, S1, and actin-S1 complex obtained from the Brookhaven Protein Database (Holmes et al., 1990; Lorenz et al., 1993; Rayment et al., 1993a, b; Mendelson and Morris, 1997) or from the Internet (Holmes et al., 2002) were approximated at different resolution by spheres of uniform, but different, electron densities using a program kindly provided by Dr. Gihan de Silva (The Randall Institute, King's College, London). In the most detailed model, which was used as a reference, spheres of 0.3 nm radius corresponding to individual amino acids were used. We found that a model with 1-nm-radius spheres where an actin monomer and S1 are represented by 9 and 30 spheres, respectively, provides a resolution of ~12 nm with a correlation coefficient of the Fourier transform, $r > 0.998$. This model was used for calculation of the intensities of the first 15 layer lines, i.e., up to 214.5 nm/15 = 14.3 nm, but it did not provide reasonably good accuracy for the layer lines with higher orders, l. For the layer lines with l from 16 up to 50, a more detailed model consisting of 47 and 145 spheres of 0.6 nm radii for actin and S1, respectively, was used. This model provides a 4-nm resolution with a correlation coefficient of the Fourier transforms, $r > 0.999$, but results in correspondingly longer computational times. These intermediately detailed sphere models corresponding to three available high-resolution structures of the actin-S1 complexes and for the "anti-rigor" model, where the light chain domain of a myosin head is tilted as a rigid body by 70° toward the M-line, are shown in Fig. 3. The last model corresponds to the pre-powerstroke state suggested by Holmes (1997). In contrast to small-amplitude elastic "bending" of the light chain domain discussed below, the term "tilting" is used here for the high-amplitude rotation of the lever arm with respect to the converter domain.

Elastic bending of the S1 "neck"

We assumed that binding of the myosin heads to actin is accompanied by elastic bending of their necks toward their "origin" on the surface of the thick filament. To account for the bending we used a 3D version of the model of Dobbie et al. (1998), where the light chain domain of S1 was assumed to bend as a cantilever. The catalytic domain of S1 (heavy-chain residues 1-770 using the nomenclature from chicken S1 sequence, here and elsewhere) was assumed to be rigid, while the "neck" domain (heavy-chain residues 771-843 and both light chains) was allowed to bend as a rod with uniform bending stiffness (clamped at residue 770) by the moment of external force applied to the residue 829. The vector between residues 770 and 829 was taken as the cantilever axis. The displacement of each sphere was assumed to be perpendicular to the cantilever axis in the plane formed by the cantilever axis and the moment of force. The value of the displacement of each sphere was calculated as $d_{829}(3L - x)x^2/2L^3$ (McLaughlin, 1977) where $L = 8.47$ nm is the distance between residues 770 and 829 or the length of the cantilever, x is the distance between residue 770 and the projection of the sphere center on the cantilever axis, and d_{829} is the displacement of residue 829. Displacement d_{829} was proportional to the projection of the moment of external force on the normal to the cantilever axis. The force that pulls the S1-S2 junction toward its "origin" on the backbone of the thick filament was assumed to be a vector having axial projection $k_z\Delta z$ and transversal projection $k_t\Delta t$ (Fig. 2). The absolute value of the displacement, d_{829}, was limited by a certain value d_{max}, which was varied from 2 to 4.5 nm to avoid unrealistically high bending of the S1 neck.

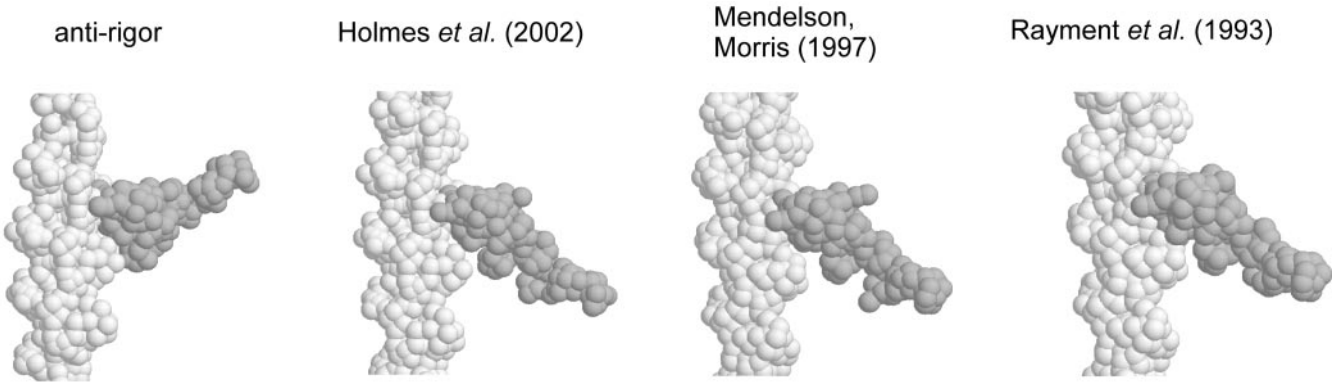

FIGURE 3 Sphere models of the actin-S1 complex obtained from the structures proposed by Rayment et al. (1993b), Mendelson and Morris (1997), and Holmes et al. (2002). The "anti-rigor" structure was obtained from the structure of Holmes et al. (2002) by 70° tilting of the light chain domain (heavy chain residues 770–843 and both light chains) toward the M-line of the sarcomere in the plane parallel to the filament axis. An actin monomer and myosin head were represented by 47 and 145 partially overlapping spheres, respectively, with 0.6 nm radii.

Lattice disorder

Although actin and myosin filaments in the overlap zone of sarcomeres form a hexagonal super-lattice, this lattice is usually significantly disordered. For this reason, in rigor or during active contraction, lattice sampling is seen only on some layer lines close to the equator, i.e., with low index l. The lattice disorder is induced by true Brownian motion of the filaments and by cross-bridge forces pulling the filaments both transversally and axially in a pseudo-random manner. Myosin filaments are kept in the lattice points by M-line proteins, which can be considered elastic elements that resist radial and axial displacement of the filaments with respect to their neighbors. Such neighbor-to-neighbor elastic interaction induces lattice disorder of the second kind, which can be described by two parameters: root-mean-square (r.m.s.) deviations in radial (Δr_T) and axial (Δz_T) positions of the central myosin filament in neighboring unit cell with respect to their position in a given unit cell (Fig. 4, Vainstein, 1963). For actin filaments, myosin heads are the only bonds keeping them in the trigonal lattice position, so that their transversal deviation from the lattice points is generally higher than that of the myosin filaments. This actin disorder is the disorder of the first kind, and can also be characterized by two parameters: r.m.s. deviations in the radial (Δr_A) and axial (Δz_A) position of actin filaments from their lattice points in a unit cell (Fig. 4, Vainstein, 1963). As axial compliance of the thin and thick filaments is very small (Huxley et al., 1994; Wakabayashi et al., 1994), axial distortion in translation of the unit cell was neglected. Although torsion compliance of the thick and thin filaments and of the proteins that keep them in Z- and M-lines is not known, we assumed that this compliance is sufficiently high and any rotation disorder can be neglected. We also assumed that disordered filaments remain parallel to the fiber axis and did not consider any tilting or bending filament disorder. Fig. 4 schematically shows the meaning of all four parameters describing lattice disorder allowed in the model.

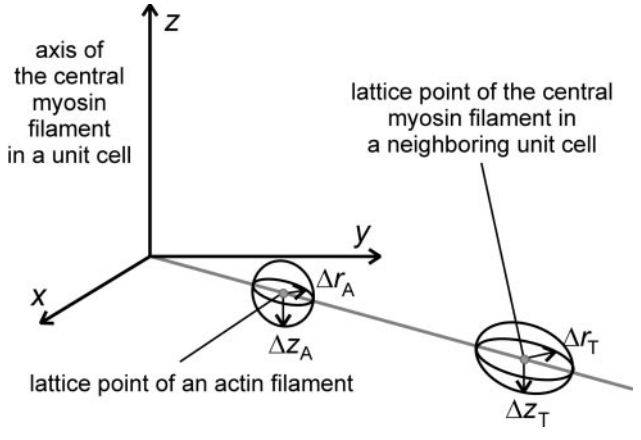

FIGURE 4 Scheme of the lattice disorder used in the model. Transversal, Δr_A, and axial, Δz_A, root-mean-square (r.m.s.) deviations of an actin filament from ideal lattice point in a unit cell describe the disorder of the first kind. Transversal, Δr_T, and axial, Δz_T, r.m.s. deviations from the ideal hexagonal super-lattice point of the central myosin filament of a neighbor unit cell characterize the disorder of the second kind. All four deviations were assumed to obey Gaussian distribution.

Intensity calculations

The intensity calculation was limited by low angles, $|Z|$, $|R| < 0.2$ nm^{-1}, where Z and R are axial and radial coordinates in reciprocal space. Contributions from the myosin backbone and myosin S2 to the x-ray diffraction pattern were neglected and not taken into account. We also did not take into account contributions of the regulatory proteins of the thin filaments. These proteins contribute to the first and second actin layer lines at the higher reciprocal radii R than myosin heads bound to actin (Kress et al., 1986; Yagi, 1991). At low $|R| < 0.15$ nm^{-1}, where calculated intensities were compared with experimental data, contributions of the regulatory proteins are probably not significant.

At first, all 270 myosin heads in the unit cell were attached to six actin filaments according to the principle of minimal elastic distortion energy with a certain value of parameters $e = k_t/k_z$ and z_0. After that, the light chain domains or "necks" of the heads were bent toward their "origins" on the backbones of the thick filaments, as described above. The intensities of the layer lines were calculated using formulas described in Appendix A.

Contribution of the Bessel functions of the first kind up to ±20th order were taken into account. To check that this limitation does not reduce the accuracy of our calculations, the Bessel functions up to ±80th were used in some test calculations. This did not affect calculated intensities, although it led to a significant increase in computational times. To reduce calculation time, a lookup table of the Bessel functions with the step of 0.05 was placed in computer memory. On an 850 MHz PC, calculation of one layer line took 15 min for the intermediate sphere model and 5 min for the model where actin monomer and myosin S1 were approximated with spheres of 1 nm radius.

For actin layer lines A1, A2, . . . corresponding in our model to the layer lines with indexes $l = 6m$ (m is integer) the intensity diffracted by isolated

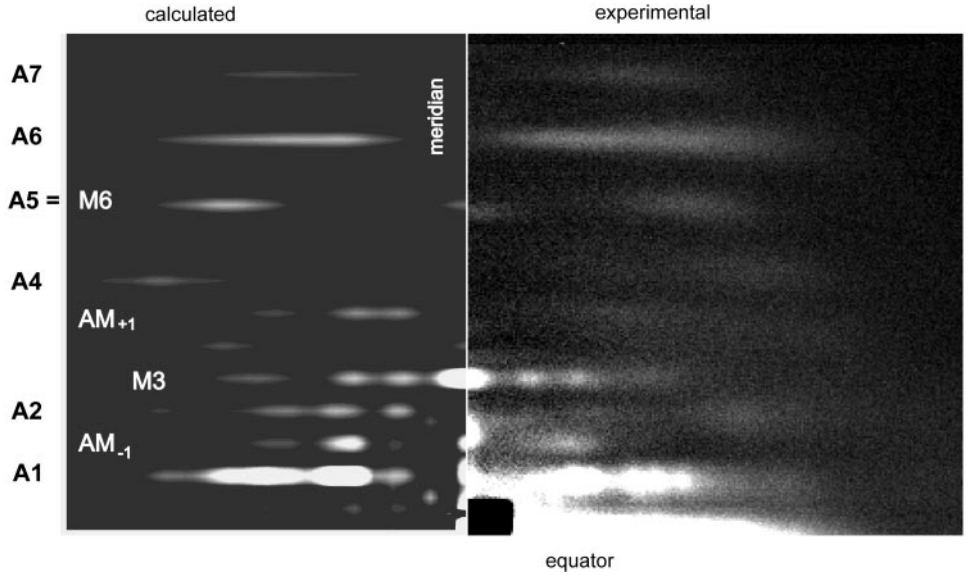

FIGURE 5 Calculated (*left*) and experimental (*right*) 2D diffraction patterns. The experimental pattern was collected from a bundle of seven rabbit muscle fibers in rigor with a total exposure of 200 s. The brightest layer lines are marked. The calculated diffraction pattern was obtained from the "reference" model described in the text.

actin filaments without bound heads was also calculated. This intensity was then added to the layer line intensity with a factor of 0.52. The factor corresponds to the contribution of the non-overlapped zone (385 nm at sarcomere length 2.4 μm) of the actin filaments to the intensity diffracted by their 735-nm-long overlapped parts (385/735 $\approx$ 0.52). As in the non-overlap zone, the hexagonal lattice transforms into a tetragonal array (Squire and Harford, 1988), it was assumed that x-rays diffracted by these two parts of the actin filaments do not interfere.

RESULTS

An experimental 2D diffraction pattern obtained from a bundle of seven rabbit muscle fibers in rigor is shown in Fig. 5. There is a characteristic set of the actin layer lines A1, . . . , A7, which are bright in rigor where myosin heads are stereospecifically bound to actin and decorate the actin helix. Substantial intensity is seen on the myosin layer lines M3 and M6, with strong meridional reflections. The spacing of the M6 reflection and that of the A5 layer line are close, although the off-meridional part of A5 is 2.5% further from the center of the image. This difference characterizes the accuracy of our approximation that five pitches of myosin helix are equal to six pitches of actin helix. Apart from the actin and myosin layer lines, two "beating" actin-myosin layer lines AM_{-1} and AM_{+1} (Huxley and Brown, 1967; Bordas et al., 1993; Yagi, 1996), are seen at $(\sim 24\ \text{nm})^{-1}$ and $(\sim 10\ \text{nm})^{-1}$, respectively. Prominent lattice sampling is seen on the first actin layer line, A1, where reflections up to (3, 0) can be distinguished. On the actin and "beating" layer lines with higher indexes, lattice sampling is hardly seen, if present, although the (1, 0) and (1, 1) equatorial reflections are markedly sampled on the M3 myosin layer line. The left half of Fig. 5 shows a 2D diffraction pattern calculated for a "reference" model with a certain set of parameters that provided a reasonably good data fit. This set was estimated from direct parametric analysis without recourse to global or local parameter search. The computer simulation of the effects of different parameters describing lattice disorder, binding patterns of the myosin heads, and configuration of the actin-myosin complex is described below.

Effect of lattice disorder on layer line intensities

The most sampled first actin, A1, and third myosin, M3, layer lines have indexes $l = 6$ and $l = 15$, respectively, in our model (Fig. 5). Lattice sampling decreases with the increase in index l of the layer line and at $l > 20$ is not seen anywhere except meridian. Fig. 6 illustrates the dependence of the intensity of the most sampled layer lines A1 and M3 on parameters characterizing lattice disorder. In the absence of any interference between x-rays scattered by different actin filaments, calculated A1 is smooth, with a broad peak at reciprocal radii $R \approx 0.045\ \text{nm}^{-1}$, which is close to the radial position of the (1, 1) equatorial reflection (Fig. 6 *A*, *dash-dot line*). If only one unit cell was taken into account, i.e., translation of the unit cells into the lattice was not considered, calculated A1 intensity profile has several broad peaks (Fig. 6 *A*, *dashed line*), but could not reproduce sampling of the lattice reflections (*h*, *k*, 6). A reasonably good fit of observed A1 was achieved if the r.m.s. of transversal translation disorder Δr_T was set to 3.5 nm and actin disorder within a cell Δr_A was set to 1 nm (Fig. 6 *A*, "reference" model, *solid line*). A further decrease in translation disorder leads to a further increase in the A1 sampling, which in this case becomes more pronounced than observed experimentally (Fig. 6 *A*, *dotted line*). As the limit, at Δr_T approaching zero, only crystalline Bragg reflections (*h*, *k*, 6) remain in the A1 layer line. Although the shape of the A1 layer line is very sensitive to the transversal disorder,

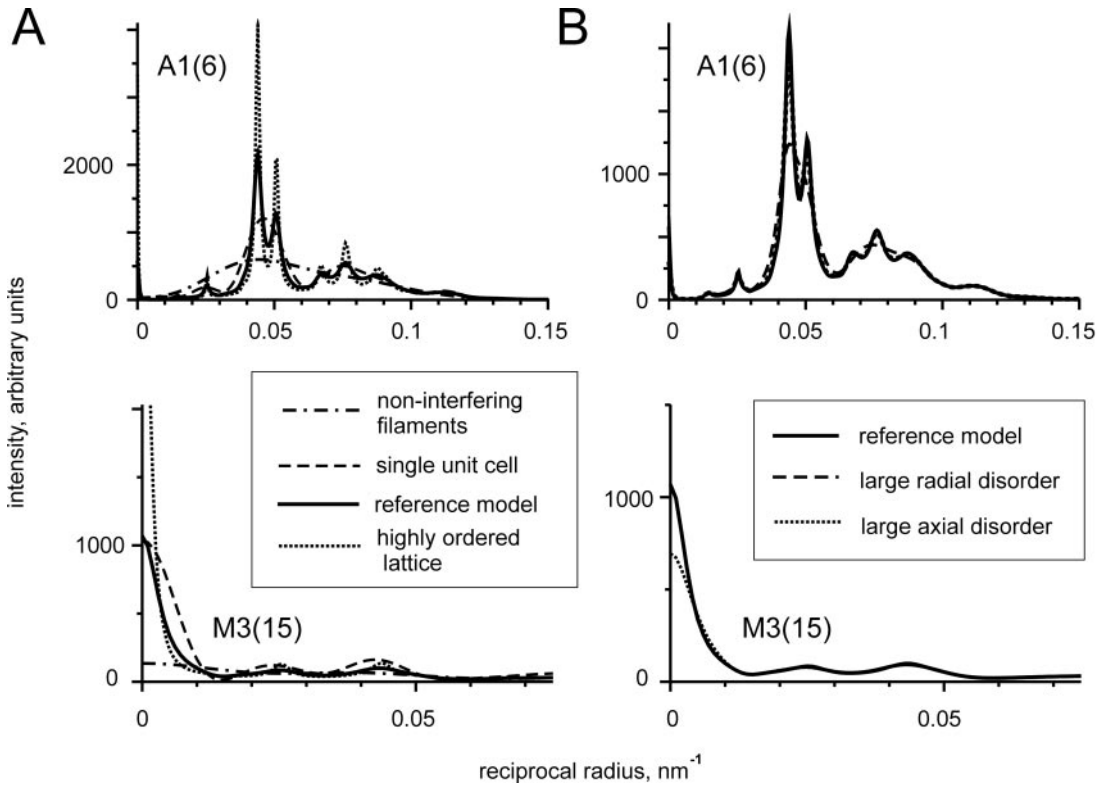

FIGURE 6 Effect of disorder parameters on calculated intensities of the A1 (*upper plots*) and M3 (*lower plots*) layer lines. (*A*) "Reference" model (Δr_A = 1 nm, Δz_A = 1.5 nm, Δr_T = 3.5 nm, Δz_T = 4.5 nm, *solid lines*); a single unit cell (Δr_A = 1 nm, Δz_A = 1.5 nm, translation of the unit cells into the lattice was not taken into account, *dashed lines*); a single unit cell without interference between the filaments (Δr_A = 10 nm, Δz_A = 10 nm, *dash-dot lines*), and a highly ordered lattice (Δr_A = 1 nm, Δz_A = 1.5 nm, Δr_T = 2.5 nm, Δz_T = 3. nm, *dotted lines*). (*B*) Effect of axial and transversal translation disorder on the layer line intensities: "reference" model (*solid lines*); high axial disorder (Δr_A = 1 nm, Δz_A = 1.5 nm, Δr_T = 3.5 nm, Δz_T = 5.5 nm, *dotted lines*); high transversal disorder (Δr_A = 1 nm, Δz_A = 1.5 nm, Δr_T = 7 nm, Δz_T = 4.5 nm, *dashed lines*). The solid and dashed lines coincide in the lower graph in *B*. For all calculations d_{max} = 2 nm and e = 0.1, "forced pairs" case, actin-S1 configuration as suggested by Holmes et al. (2002).

it is much less sensitive to the axial disorder either within a unit cell or in the unit cell translation (Fig. 6 *B*).

At Δr_A = 0.5–1.5 nm, the sampling of the (1, 0) and (1, 1) equatorial reflections similar to that observed experimentally (Fig. 5) is clearly seen on the calculated M3 layer line (l = 15) even if translation of the unit cell is not taken into account (Fig. 6 *A*). A further increase in Δr_A eliminates the sampling. Changes in transversal lattice disorder, however, do not affect calculated meridional intensity on the M3 layer line (Fig. 6 *B*). An increase in axial translation disorder Δz_T decreases meridional intensity on the M3 layer line, but does not affect its off-meridional part and the A1 intensity (Fig. 6 *B*). Alternatively, an increase in transversal translational disorder Δr_T significantly decreases lattice sampling on the A1 layer line, but practically does not affect the M3 intensity (Fig. 6 *B*). Values of Δz_A = 1.5 nm and Δz_T = 4.5 nm were found to provide reasonably good fit for both M3 and M6 meridional reflections in our experimental pattern (Fig. 5). Values of Δr_A = 1 nm, Δz_A = 1.5 nm, Δr_T = 3.5 nm, Δz_T = 4.5 nm were taken for our "reference" model.

The most remarkable result of the calculations is that the total off-meridional intensity of a layer line is practically independent of lattice disorder. The total intensity of the A1 layer line changes by <2% when Δr_A increases from 1 nm to 10 nm if only one unit cell was taken into account (Fig. 6 *A*). Even for the most sampled case shown in Fig. 6 *A* (*dotted line*), which is oversampled compared to observed patterns, the total off-meridional A1 intensity was 99.6% of that calculated for the reasonably sampled "reference" model. The total off-meridional A1 intensity for the "reference" model was 98% of the total intensity calculated for a single unit cell with the same disorder parameters Δr_A, Δz_A (Fig. 6 *A*, *solid* and *dashed lines*).

The actin labeling pattern and its effect on diffraction intensity

Fig. 7 shows an example of calculated distribution of 270 myosin heads on six actin filaments obtained with the principle of minimal elastic distortion energy for stiffness ratio e = 0.1, assuming that two heads of a myosin molecule are forced to bind actin monomers on the same thin filament ("forced pairs" case). On an actin filament, myosin heads

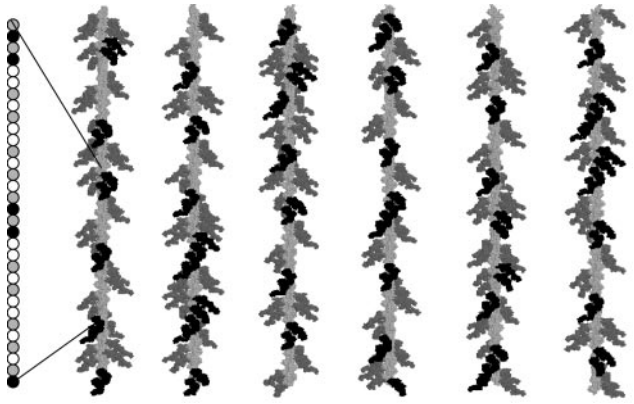

FIGURE 7 An actin labeling pattern obtained using the principle of minimal distortion energy for a "forced pairs" case of the rigor model with the stiffness ratio $e = k_t/k_z = 0.1$. All six actin filaments in a hexagonal super-lattice unit cell with attached myosin heads are shown as they are seen from the center of the cell. Dark myosin heads project from the central myosin filament, while the light ones originate from the distal myosin filaments in the cell. The Z-line is in the bottom of the picture. The inset on the left schematically shows the binding pattern on a fragment of an actin filament: open circles represent actin monomers not occupied by bound heads, filled circles correspond to actin sites occupied by myosin heads from the central myosin filament. Actin monomers with bound myosin heads that originate from other myosin filaments are shown in gray.

originating from one thick filament tend to form "target zones" (Haselgrove and Reedy, 1978; Squire and Harford, 1988) separated by one ~36 nm pitch of the actin helix.

Although in the "free choice" case two heads of a myosin molecule were allowed to bind different actin filaments, for a majority of 55–66% (at $e = 0.1$ and $e = 1$, respectively) of the myosin molecules, both heads prefer to bind two adjacent monomers on an actin filament, as in the "forced pairs" case. The standard deviation of the axial displacement of the S1-S2 junction, Δz, increased from 3.2 nm at $e = 0.1$ to 4.5 nm at $e = 1$. Average Δz was in the range of −0.3 nm to 0.4 nm, depending on e and z_0, showing that the positive and negative forces approximately cancel out.

As shown in the previous section the total off-meridional intensity of a layer line does not depend on lattice sampling, and therefore is mainly determined by diffraction on an actin filament decorated with bound myosin heads. Intensity diffracted by such a decorated helix depends on the binding pattern. Although in our model the light chain domains of individual myosin heads can bend toward their "origin" on the backbone of the thick filaments, an actin filament decorated by stereospecifically bound myosin heads can be approximated by a partially occupied helix, i.e., by a set of identical myosin heads bound to some, but not to all, discrete points of the actin helix. For such a structure diffracted intensity can be calculated straightforwardly (Appendix B). As seen from Eq. B2, the intensity diffracted by such a structure is fully determined by the Fourier-Bessel structural factors of a single myosin head bound to actin and the

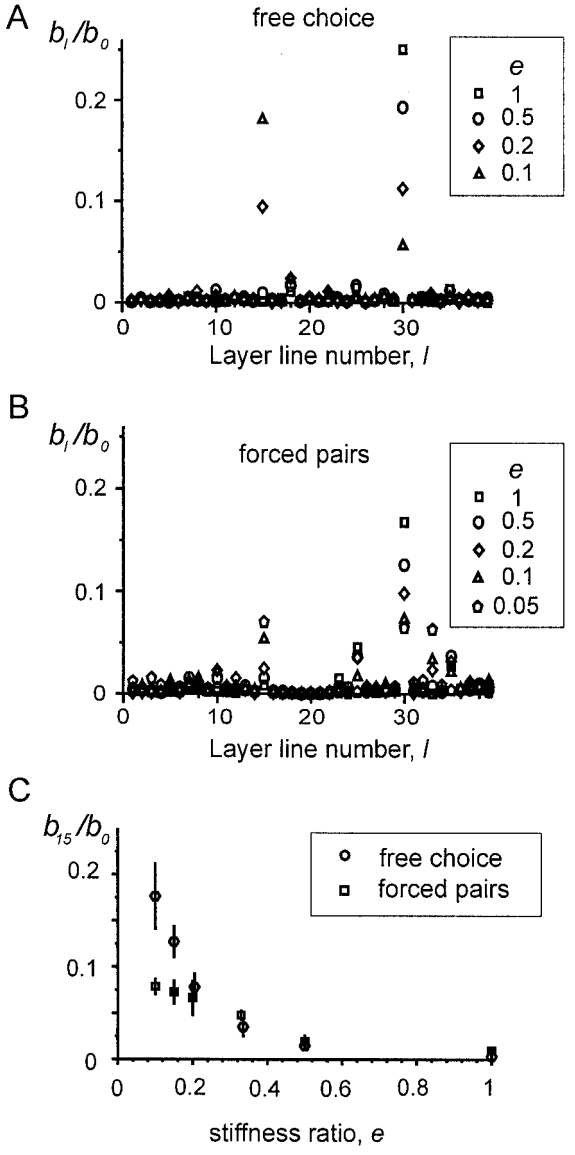

FIGURE 8 Normalized one-dimensional interference function B for several actin labeling patterns calculated using the principle of minimal elastic distortion energy for the "forced pairs" (*A*) and "free choice" (*B*) cases at different e (e values are shown in the inset). As function B is even and has a period of 78, only b_l values up to $l = 39$ are shown. In *C*, b_{15}/b_0 is plotted against e for both cases. Vertical bars show maximal and minimal values of b_{15}/b_0 obtained at various shifts between actin and myosin filaments, z_0.

parameters b_1 (Eq. B4, B5) of the one-dimensional interference function $B(Z)$. This function characterizes the binding pattern of the myosin heads to actin.

We first consider what kind of interference functions $B(Z)$ one can obtain using the principle of minimal elastic distortion energy and then estimate how the binding pattern affects the intensities of different layer lines. Fig. 8 shows interference function $B(Z)$ at different values of the stiffness ratio e for the cases of "free choice" (Fig. 8 *A*) and "forced pairs" (Fig. 8 *B*). In both cases the most prominent peaks are

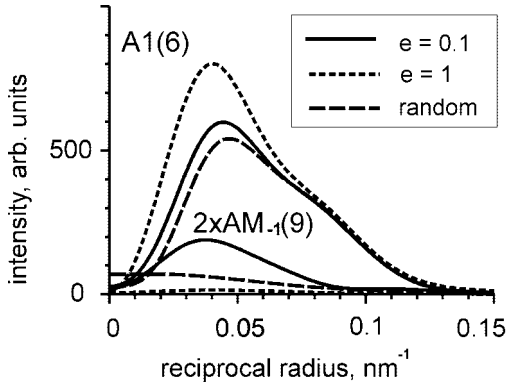

FIGURE 9 Effect of the actin binding pattern on calculated intensities of the A1 and AM_{-1} layer lines (numbers l are shown in parentheses). Calculations were done for the "forced pair" case with $e = 1$, $e = 0.1$, and for a random distribution of bound myosin heads on actin filaments (the meanings of the different lines are shown in the *inset*). Only one single unit cell without interference of the x-ray diffraction from different filaments ($\Delta r_A = 10$ nm, $\Delta z_A = 10$ nm) was considered. The AM_{-1} intensities were multiplied by a factor of 2 for better visualization.

seen on the 15th and 30th layer lines, which correspond to the 14.3 nm repeat of the crowns of myosin heads on the thick filament and to the greatest common measure of the pitches of the actin and myosin helices (7.15 nm = 35.75 nm/5, 7.15 nm = 42.9 nm/6). The appearance of these peaks indicates that for any e binding pattern predicted by the principle of minimal elastic distortion, energy is not random and is strongly modulated by myosin-based periodicities. The interference function $B(Z)$ depends not only on parameter e, but also on the shift between the actin and myosin filaments z_0. The full variations of b_{15} for the whole range of z_0 between 0 nm and 35.75 nm are shown in Fig. 8 *C* at each e, together with their average values. Changes in z_0 by several nanometers induces nearly full-scale variation in b_l. As the length of individual sarcomeres may vary slightly, even in highly ordered muscle fibers, effective b_l is its average over z_0. Only these average values of b_l are plotted in Fig. 8, *A* and *B*.

When e decreases (this means that axial stiffness of a cross-bridge becomes higher than its transversal stiffness), b_{15} increases at the expense of b_{30} (Fig. 8, *A* and *B*), because axially stiff cross-bridges tend to bind actin monomers with minimal deviation from the myosin-based 14.3 nm repeat. For any given e the "free choice" model, where the myosin heads are less restricted and can bind to more convenient sites, provides a higher value of b_{15} than the "forced pairs" model (Fig. 8, *A* and *B* and *C*). Variations in z_0 mostly affect the interference function in the "free choice" case at $e \leq 0.15$.

As follows from the theory described in Appendix B, the Fourier-Bessel terms G_{nl} not satisfying the conventional helix selection rule ($l = nT + mU$; Cochran et al., 1952) contribute to a layer line intensity I_l. Fig. 9 demonstrates that such a contribution can be significant. Calculated intensities of the A1 layer line for the "forced pairs" case are plotted at $e = 0.1$, $e = 1$ and for a random distribution of the myosin heads on the thin filaments. In the last case, b_{30} is very small and the A1 intensity is mainly determined by the contribution of the main term, b_0. At $e = 0.1$ the total A1 intensity, I_{A1}, is 10% higher than that for random distribution of the heads (Fig. 9). At $e = 1$ when b_{30} is ~17% of b_0 (Fig. 8 *B*), I_{A1} is higher than that for the random distribution by a factor of 1.41.

An increase in e leads to a decrease in the AM_{-1} intensity (Fig. 9), and in the AM_{+1} intensity (not shown) coming from the contribution of b_{15} (see Appendix B). This occurs because of reverse changes in b_{15} and b_{30} (Fig. 8, *A* and *B*) so that a decrease in b_{30} leads to a decrease in the A1 intensity, while an increase in b_{15} gives rise to the AM_{-1} and AM_{+1} intensities. The sum of the A1, AM_{-1}, and AM_{+1} intensities remains constant within 5% error, while the intensity of A1 alone increases by 28% when e varies from 0.1 to 1. Similar features, i.e., redistribution of the intensity from A1 to the "beating" layer lines, AM_{-1} and AM_{+1} at a nearly constant sum of their total intensities, were found for the "free choice" case of our model. As changes in e lead to a intensity redistribution between the A1 and beating layer lines, the ratio of their intensities can be used for estimation of e. For random distribution of the heads on actin, a significant amount of the intensity is spread over other layer lines, i.e., in the background. As a result, the sum of the A1, AM_{-1}, and AM_{+1} intensities is ~20% less than that for all models based on the principle of minimal elastic distortion energy.

Although some contribution of the J_2 Bessel function to the A6 and A7 layer lines is predicted by the theory developed in Appendix B, calculations show that this contribution is negligible and the intensities of these layer lines are independent of the distribution of bound myosin heads on the thin filaments. This is probably because the main helical term on these layer lines is proportional to J_1 and predominates over all others. We have not found any statistically significant difference in the interference function $B(Z)$ and in the calculated diffraction pattern between the superlattice and simple lattice structures of the A-band either for the "free choice" or "forced pairs" case (not shown).

Effect of bending myosin necks

For a reasonable range of disorder parameters, lattice sampling on the sixth and seventh actin layer lines, A6 and A7 ($l = 36, 42$) is negligible. If it is assumed that all actin-S1 complexes in rigor have the same configurations as they were found in the in vitro experiments (Rayment et al., 1993b; Mendelson and Morris, 1997; Holmes et al., 2002), our model predicts a two-hump radial distribution of the x-ray intensity on the A6 (Fig. 10) never seen experimentally. This feature of the intensity distribution does not

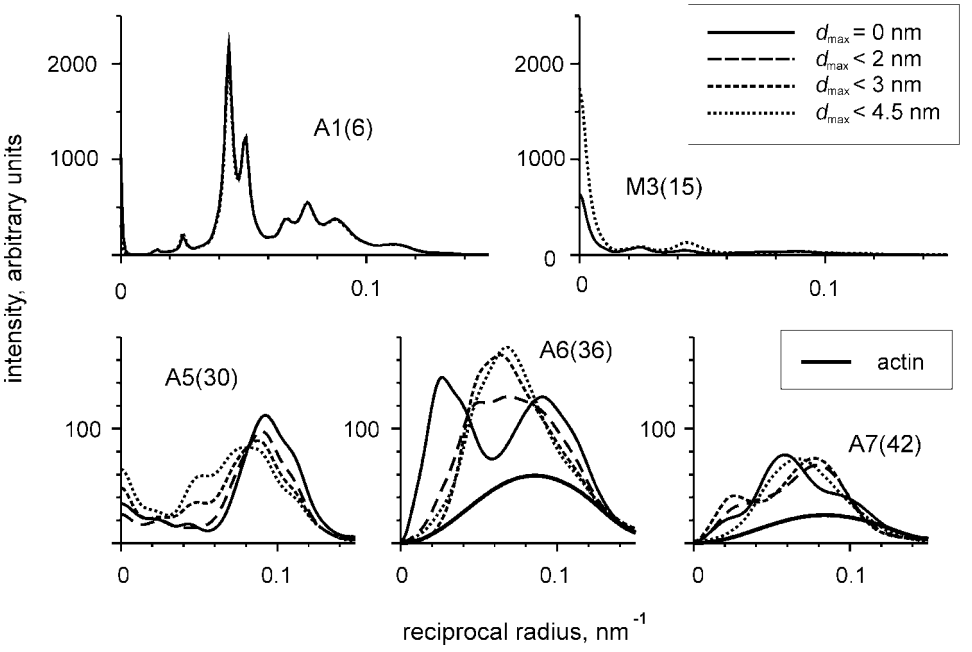

FIGURE 10 Effect of elastic bending of the light chain domains ("necks") of the myosin heads on calculated layer line intensities. The layer line numbers *l* are shown in parentheses. The "necks" of the myosin heads were assumed to bend by elastic force toward their origin on the backbone of the myosin filament. Elastic displacement of the distal end of the head was limited by a certain value d_{max}. Calculations made with various d_{max} values are shown by the lines specified in the inset. Calculated diffraction intensities of the A6 and A7 layer lines for actin filaments without bound myosin heads are also shown (*bold solid lines*). All other parameters were as in the "reference" model (see legend to Fig. 6).

depend on the actin labeling pattern and occurs because of interference between the x-rays diffracted by the actin helix and by the myosin heads attached to it. This effect of interference should diminish if the light chain domains or the "necks" of the myosin heads are disordered. According to the findings of Dobbie and colleagues (1998), we assumed the "neck" domains of the myosin heads can be bent by applied force toward its "origin" on the backbone of the thick filament, but the displacement of the distal part of the light chain domain is limited by a certain value d_{max}. Fig. 10 shows the intensity profiles of some layer lines calculated at different d_{max}. The intensity profiles of the A6 and A7 layer lines become one-humped at $d_{max} \geq 2$ nm (Fig. 10). At $d_{max} = 2$ nm the profiles of the A5, A6, and A7 layer lines are mostly similar to experimental data. Calculated A1 intensity is almost unaffected by bending of the "neck" domains, while the intensity of the M3 myosin layer line increases significantly, as the "necks" bent toward their "origin" on the myosin backbone better follow the 14.3 nm axial repeat (Fig. 10). A similar, but slightly less satisfactory, result was obtained by simply assuming that the "neck," i.e., the light chain domains of the heads, are randomly bent by Brownian-like forces.

Effect of the shape of the actin-myosin complex on layer line intensities

The results of the calculation of layer line intensities for different configurations of the actin-S1 complex shown in Fig. 3 are presented in Fig. 11. All lattice disorder parameters, d_{max} and *e* were the same, and corresponded to the "reference" model. The total integral intensity of the A1 layer line was the same within 3% for all configurations tested. The intensity of the M3 myosin layer line was also approximately the same, except for the "anti-rigor" configuration where the "neck" domain of the heads was tilted toward the M-line by 70° with respect to its position in rigor. In the last case, the M3 intensity is much higher than for other configurations because the electron density of the heads is less spread along the fiber axis. The 70° tilting of the "necks" induces shift of the intensity peaks on both the A6 and A7 actin layer lines toward meridian compared to rigor models. Other models of the actin-S1 complex provide intensity distribution on the A5, A6, and A7 layer lines qualitatively similar to those observed experimentally (Figs. 5, 13). It should be emphasized that even minor changes in the shape of bound heads, which are hardly seen by eye in Fig. 3, induce significant changes in the intensities of the A5, A6, and A7 actin layer lines (Fig. 11).

Stretch of rigor muscle fibers induces an increase in the intensity of the M3 meridional reflection (Bershitsky et al., 1996; Dobbie et al., 1998) and a less marked increase in the intensity of the M6 meridional reflection (Takezawa et al., 1999). These observations quantitatively agree with the assumption that the "neck" domain of the heads bends as a cantilever (Dobbie et al., 1998). We modeled the effect of stretch of rigor muscle by applying additional bending to the S1 "necks" by 1 nm directed toward the M-lines. The result of the calculations is shown in Fig. 12. As in the cited experiments, stretch induced a significant increase in calculated meridional intensities on the M3 and a slightly smaller increase on the M6 layer lines, while the intensities of other layer lines practically did not change.

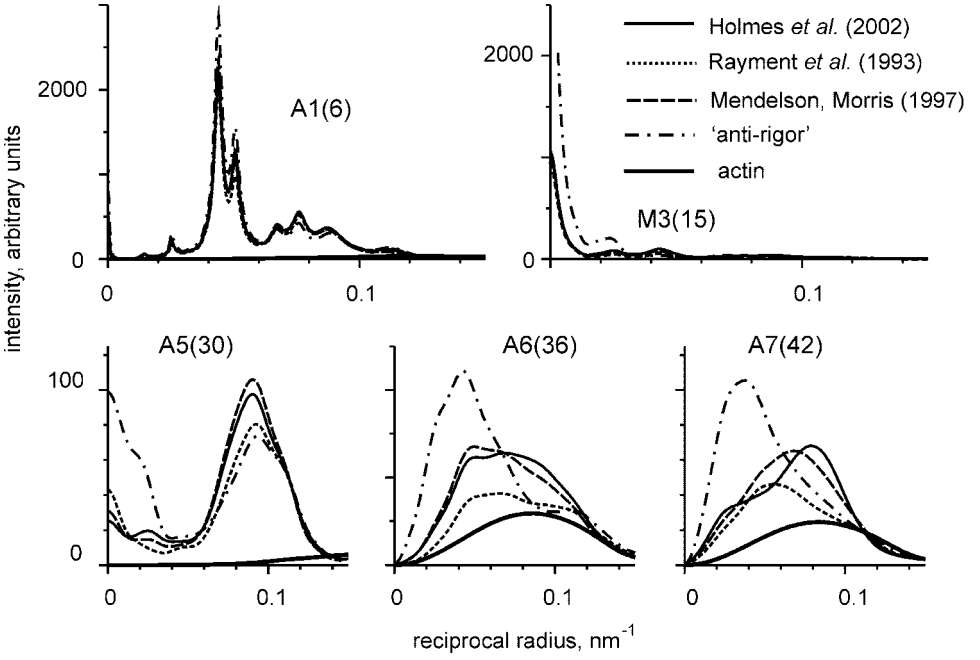

FIGURE 11 Calculated intensities of some actin and myosin layer lines for a set of configurations of the actin-S1 complex shown in Fig. 3. For all configurations e, d_{max}, and lattice disorder parameters were the same as for the "reference" model (see legend to Fig. 6). Bold solid lines show calculated diffraction from actin filaments without bound myosin heads. The meanings of the other lines are explained in the inset.

Comparison with experimental data

Results of the calculation of the 2D diffraction pattern for the "reference" model are shown together with experimental pattern in Fig. 5. The actin labeling pattern for this model was obtained using the principle of minimal distortion energy for the "forced pairs" case with $e = 0.1$ at a z_0 value that provides average b_{15}. In the "reference" model the configuration of the actin-S1 complex suggested by Holmes et al. (2002) was used, as it provides highest ratio of the A6 and A1 intensities among other available structures. The "necks" of the myosin heads were allowed to bend toward their "origin" on the backbone of the myosin filaments by not more than 2 nm. The values of $\Delta r_A = 1$ nm, $\Delta z_A = 1.5$ nm, $\Delta r_T = 3.5$ nm, $\Delta z_T = 4.5$ nm were chosen because they provide reasonably good fit of the intensity profiles along the A1, M3, and M6 layer lines estimated by eye. No further attempt was made to improve the fit using a parameter search because our goal was to estimate the effect of dif-

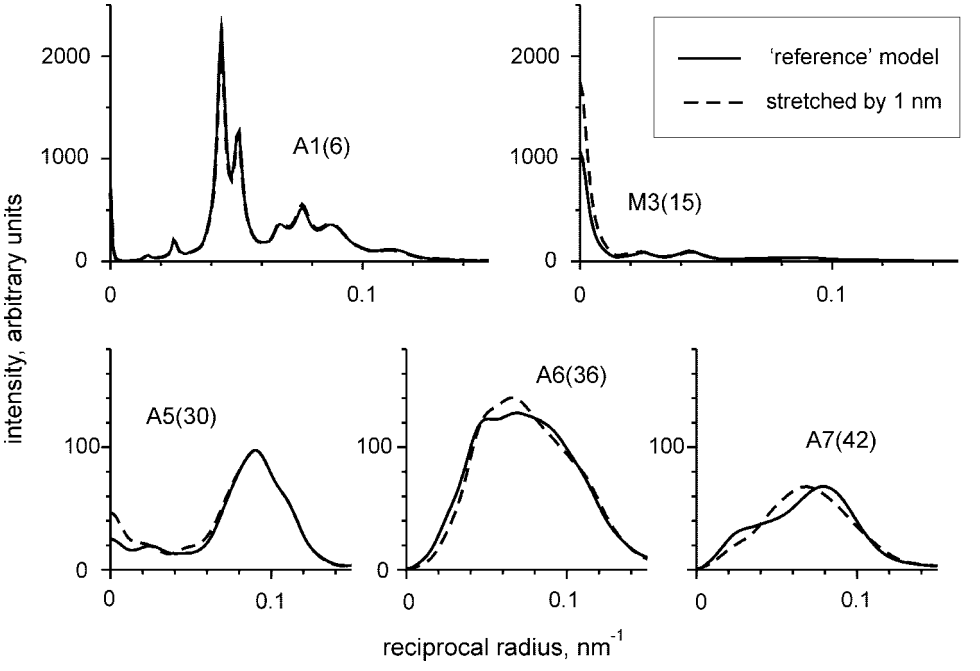

FIGURE 12 Effect of "stretch" on calculated layer line intensities. Stretch of rigor muscle was modeled by additional elastic bending of the distal parts of the myosin heads by 1 nm toward the M-line. Other parameters were the same as in the "reference" model.

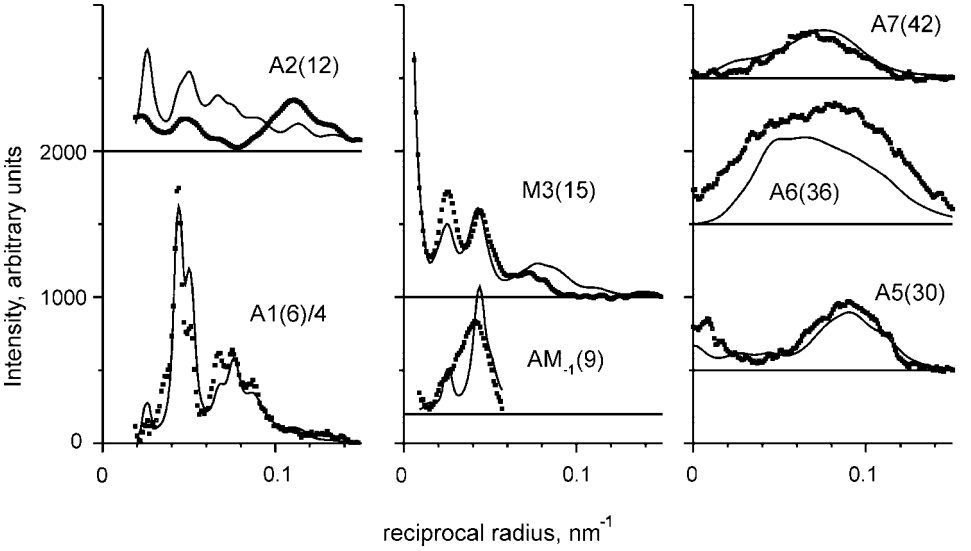

FIGURE 13 The intensities of the brightest layer lines measured experimentally (*points*) and calculated for the "reference" model (*solid lines*). Experimental data are the same as shown in Fig. 5. Layer line numbers are shown in parentheses. Calculated intensities of all layer lines were scaled with a factor providing best fit of the experimental data. Calculated and observed intensities of the first actin layer line A1 are divided by a factor of 4.

ferent parameters on the diffraction pattern, not to achieve best fit of a particular set of data. The intensity profiles calculated for this "reference" model and found experimentally are shown in Fig. 13.

The quality of the fit was estimated using the square *R*-factor, R_f, calculated as $R_f = \Sigma_i (I_i^e - I_i^c)^2/\Sigma_i (I_i^e)^2$, where I^e and I^c are experimental and calculated intensities. For the "reference" model R_f was 6.9%. The only layer line that looks significantly different from the experimental one is A2. If this layer line was eliminated, R_f decreased to 6.4%.

Although the quality of the fit was quite satisfactory, we found some difficulties in quantitative modeling of the A6 and A7 layer lines. First, we found that the F-actin models of Holmes et al. (1990) and Lorenz et al. (1993) are not good for approximation of the thin filament in rabbit muscle. Indeed, the ratio of the integrated intensities of the A7 and A6 layer line for these models is ~0.4, while in our patterns collected from relaxed rabbit muscle fibers it was ≤0.18. Another problem is that the ratio of the integrated A6 and A1 intensities in rigor muscle is higher than that predicted by the model based on any available actin-S1 structure. The best fit of the experimental A1, A6, and A7 layer lines in rigor was obtained with the model of Holmes et al. (2002), but even it underestimates the observed intensity ratios I_{A6}/I_{A1} and I_{A7}/I_{A6} (Fig. 13). The ratio of the total integral intensities of the A6 and A1 layer lines I_{A6}/I_{A1} for the pattern shown in Fig. 5 is 0.35, while for the models of Mendelson and Morris (1997) and Holmes et al. (2002) it is 0.23 and 0.25, respectively. An even smaller intensity ratio (0.17) was obtained with the original model of Rayment and colleagues (1993b). Also, all three models predict a higher ratio of the A7 and A6 intensities than its experimental value. For the pattern shown in Figs. 5 and 13 this ratio is 0.26, while for the models of Rayment et al. (1993b), Mendelson and Morris (1997), and Holmes et al. (2002) it is 0.52, 0.47, and 0.43, respectively.

DISCUSSION

The direct modeling described here is based on available atomic structures of F-actin (Holmes et al., 1990), S1 (Rayment et al., 1993a) and of the actin-S1 complex (Rayment et al., 1993b; Mendelson and Morris, 1997; Holmes et al., 2002) and on a simple physically plausible rule for selection of an actin binding site for each myosin head. Calculations presented in Figs. 5 and 13 demonstrate that despite its simplicity, this approach provides a good quantitative fit of the whole 2D x-ray diffraction pattern from skeletal muscle in rigor, although no parameter search was carried out to improve the quality of the fit. Our goal was not to achieve the best fit of a particular set of data, but rather to obtain a quantitative understanding of the effects of different parameters describing actin labeling pattern, lattice disorder, and the shape of the actin-S1 complex on observed diffraction intensity.

Principle of minimal elastic distortion energy and actin labeling pattern

With this principle a single dimensionless parameter, the ratio of transversal and axial cross-bridge stiffness, *e*, completely determines which actin binding sites are occupied by myosin heads in a unit cell of the actin-myosin super-lattice in rigor. At low *e*, the actin binding pattern also depends on the axial shift between the actin and myosin filaments z_0. However, this parameter can be excluded from the model as an unavoidable variation of the sarcomere length leads to an averaging of the binding pattern over the whole range of z_0. Although the principle is very simple, it is sufficient to reproduce some key features of observed A-band structure in rigor skeletal muscle, particularly the tendency of the myosin heads originating from a thick filament to bind "target zones" on an actin filament spaced axially ~36 nm

apart, and the presence of ~14.3 nm myosin-based periodicity in the actin labeling pattern (Varriano-Marston et al., 1984).

Apart from the meridional reflection on the M3 layer line, the ~14.3 nm modulation of the binding pattern produces so-called "beating" actin-myosin layer lines AM_{-1} and AM_{+1} at ~24 nm and ~10.2 nm, respectively. Their intensities are also proportional to the b_{15} term of the interference function that quantitatively describes the modulation. These layer lines are observed in the diffraction pattern from skeletal muscle in rigor (Figs. 5 and 13; Huxley and Brown, 1967). Yagi (1996) has explained the appearance of these layer lines in the framework of the modulation theory originally suggested by Holmes et al. (1980). However, Yagi (1996) mistakenly assumed that the intensity distribution along the AM_{-1} and AM_{+1} layer lines is the same as that for the A1 layer line. As shown in Appendix B, AM_{+1} contains contributions from both the J_2 and J_1 Bessel functions, while A1 and AM_{-1} contain contributions only from J_2.

Calculations show that the ratio of the total off-meridional intensities of the A1 and AM_{-1} layer lines is independent of lattice disorder and of the shape of the actin-S1 complex. This ratio depends only on the stiffness ratio e and, therefore, e itself can be estimated directly from the observed ratio of the A1 and AM_{-1} intensities. Depending on the "free choice" or "forced pairs" case of the model, an e value of 0.1–0.2 was found to provide reasonably good agreement between the observed and calculated intensity ratio. Axial stiffness of a myosin head in rigor was found to be at least 1.5 pN/nm (Linari et al., 1998). Its radial stiffness was estimated to be ~0.5 pN/nm or less (Brenner et al., 1996). These values correspond to $e \leq 0.3$, i.e., a value close to our estimation. In any case, the results of the modeling suggest that a myosin head is significantly stiffer axially than transversally.

Two different rules for binding of two heads of a myosin molecule, "free choice" and "forced pairs" cases, were tested and compared. It was found that even if two heads of a myosin molecule are allowed to bind different actin filaments, the majority of the molecules still prefer to bind two neighbor sites of an actin filament with both heads. The results of the intensity calculation do not allow distinguishing between the "forced pair" and "free choice" cases of the model from diffraction data. Although these two cases predict different relationships between e and b_{15} (Fig. 8 *C*) at any given b_{15}, the diffraction patterns calculated using two assumptions were very similar, so that no specific features that are characteristic only for one or another case were found.

In both "free choice" and "forced pairs" cases, the principle of minimal elastic distortion energy predicts not only ~14.3 nm myosin-based modulation of the binding pattern, but also a ~7.2 nm modulation, which corresponds to the greatest common measure of the pitches of the actin (~36 nm) and myosin (~43 nm) helices. In the interference function this modulation is expressed by the b_{30} term (Eqs. B4, B6). The presence of a strong meridional reflection on the M6 myosin layer line (Figs. 5 and 13) is a "mark" of this modulation. The same b_{30} term determines contribution of the "non-helical" (i.e., not satisfying the helix selection rule) Bessel functions to the intensities of the A1, A6, and A7 layer lines. As seen from Fig. 9, such contributions can be substantial for A1, if e is high.

When e decreases, b_{30} also decreases at the expense of b_{15} (Fig. 8), so that the intensities of the AM_{-1} and AM_{+1} "beating" layer lines increase at the expense of decreasing contribution of the "non-helical" Bessel functions to the A1 intensity. As a result of these inverse relationships between b_{15} and b_{30}, the sum of the total off-meridional intensities of the A1, AM_{+1}, and AM_{-1} layer lines is independent of e, and depends solely on the number of myosin heads stereospecifically bound to actin.

Actin-myosin lattice and diffraction intensity

In contrast to significant differences in the diffraction pattern of relaxed muscles with the super- and simple-lattice structure of the A-band (Huxley and Brown, 1967), no significant difference in calculated interference function and diffracted intensities was found between these two models in rigor. This means that the actin labeling pattern in rigor is not strongly dependent on a difference in the orientation of the myosin filaments.

Disorder of the filament super-lattice affects the intensities of the x-ray reflections. As it was described and explained by Huxley and colleagues (1982), axial disorder of the myosin filaments in neighboring unit cells (determined in our model by Δz_T) is the disorder of the second kind (Vainstein, 1963). This disorder leads to an increase in the radial width and to a decrease the intensity of the M3 (Fig. 6 *B*) and M6 myosin meridional reflections. Axial disorder of the thin filaments within a unit cell (Δz_T) also affects the intensities of the myosin meridional reflections, but not their width, as this is a disorder of the first kind (Vainstein, 1963). In practice, these two parameters can be estimated independently of transversal disorder from the width of the meridional reflections M3, M6, etc. However, it is difficult to estimate both these parameters with reasonably good precision and to determine quantitatively the effect of the lattice sampling on observed intensities of the myosin meridional reflections. In any case, as it is seen from the calculations presented in Fig. 6, neglecting effects of axial disorder in quantitative interpretation of these intensities (Juanhuix et al., 2001) can be a source of significant errors.

Radial distribution of the x-ray intensity along the layer lines with low indices l is very sensitive to the transversal lattice disorder, i.e., deviation of the filament positions from hexagonal lattice points in a plane perpendicular to the filament axis. Sampling of the Bragg reflections up to (3, 0)

can be seen in the A1 layer line in rigor (Figs. 5, 13; Xu et al., 1997). To account for this sampling one has to take into account translation of the unit cells into the lattice, as the sampling cannot be reproduced by a model containing only one super-lattice unit cell (Fig. 6 *A*). Sampling of the (1, 0) and (1, 1) equatorial reflections seen on the M3 layer line is mainly determined by the transversal disorder within a unit cell, Δr_A, and is not very sensitive to the translation disorder of the cell packing, Δr_T (Fig. 6). Both parameters describing transversal disorder, Δr_A and Δr_T, can be independently estimated from the shape of the A1 and M3 layer lines, as their off-meridional intensities are practically independent of axial disorder (Fig. 6). For all reasonable values of the disorder parameters any interference between the x-rays diffracted by different actin filaments is not significant for the layer lines with indexes $l > 20$, except the meridional reflections. The off-meridional intensities of these layer lines can be considered diffracted by isolated thin actin filaments with bound myosin heads.

An important result of the calculations is that the total off-meridional intensity of a layer line was found to be independent of lattice disorder and, therefore, can be considered as invariant of interfilament interference. This integral intensity depends only on the pattern of actin labeling and on the configuration of the actin-S1 complex. Of course, this conclusion is valid only if disordered filaments remain parallel to the fiber axis.

Configuration of the actin-S1 complexes and diffraction intensity

Three available structures of the actin-S1 complexes obtained by docking of the atomic structures to low-resolution EM images (Rayment et al., 1993b; Mendelson and Morris, 1997; Holmes et al., 2002) were tested, and calculated layer line intensities were compared to the experimental ones. We also tested a model where the "necks" or the light chain domains of S1 were tilted by 70° toward the M-line. Such structure is often assumed to correspond to the beginning of the "power stroke" (Holmes, 1997; Dominguez et al., 1998). Even such global change in the shape of the heads does not affect the intensities of the low-order layer lines, A1 and AM_{-1} (Fig. 11).

High-order actin layer lines in the low-angle diffraction pattern limited by ~5 nm resolution are, however, quite sensitive to ~1 nm changes in the configuration of bound myosin heads. For three "rigor" actin-S1 structures appearing similar to the naked eye, calculated intensities of A5, A6, and A7 layer lines are quite different (Fig. 11). These intensities are also very sensitive to <2 nm bending of the light chain domains of the heads (Fig. 10). The effect of small changes in the shape of the heads on diffraction intensities is also seen from the result of the calculations shown in Fig. 12. A stretch of rigor muscle was modeled by a tilting of the "necks" of the myosin heads toward the M-line. A 1-nm tilting induced an increase in the calculated meridional intensity on the M3 and M6 layer lines similar to that observed experimentally (Bershitsky et al., 1996; Dobbie et al., 1998; Takezawa et al., 1999).

Calculated and observed diffraction pattern: limitation of available high-resolution structures

Although the "reference" model provides a reasonably good fit of observed data (Figs. 5 and 13), there was some systematic difference between calculated and experimental diffraction patterns for all tested models. This difference does not depend on parameters describing actin labeling or lattice disorder in our model, and is solely induced by available high-resolution structure of F-actin, S1, and their complex. One of the goals of our work was to check whether the actin-S1 structures obtained from docking of atomic structures to EM images can indeed provide a good fit of the low-angle diffraction patterns collected from muscle fibers.

The ratio of the total intensities of the A7 and A6 layer lines calculated for F-actin structures of Holmes et al. (1990) and Lorenz et al. (1993) is ~0.4, while the same ratio for diffraction patterns collected from relaxed rabbit muscle fibers in our experiments was 0.15–0.18. A significant difference is seen in the A2 actin layer line in rigor, where the model tends to overestimate the intensity at $R < 0.1$ nm^{-1} and to underestimate it at $R > 0.1$ nm^{-1} (Fig. 13). Also, for all three actin-S1 structures calculated total A6 intensity (more specifically, its ratio to the A7 and A1 intensities) is always higher than observed experimentally.

A possible reason for such differences is the effect of tropomyosin and troponin on the structure of the actin monomers and/or their packing into F-actin. Also, these regulatory proteins can contribute to actin layer line intensities. We could not include the effects of tropomyosin and troponin in our modeling, as to date there are no available structures of the F-actin-tropomyosin troponin complex in the absence and presence of bound myosin heads. Also, the structures of the actin-S1 complex used in the modeling were obtained by docking S1 into F-actin without tropomyosin or troponin. These structures can be different from those formed in rigor muscle in the presence of these proteins.

Despite mentioned difference between calculated and observed diffraction patterns caused by limitation of our current knowledge about actin and myosin structures, results of direct modeling presented here provide some useful tool not only for analysis of rigor patterns, but also for interpretation of diffraction data collected from actively contracting muscle. The fact that the total off-meridional layer line intensity is independent of lattice sampling allows us to compare quantitatively patterns collected from the same preparation

in the conditions where the degree of crystallinity varies. Another finding is that the sum of the total off-meridional intensities of the first actin (A1) and the "beating" (AM_{-1} and AM_{+1}) layer lines is invariant under changes in the shape of the actin-S1 complexes, lattice disorder, and parameter *e* describing the actin labeling pattern. This allows us to use this sum for estimating the number of myosin heads stereospecifically bound to actin during muscle contraction under different mechanical and biochemical conditions.

APPENDIX A

Calculation of the layer line intensities

All calculations were made using cylindrical coordinates r, ψ, z, where the z-axis coincides with the axis of the central thick filament in the unit cell (Fig. 1). Fourier transforms F_{kl} on the lth layer line of kth thin filament ($k = 1, \ldots, 6$) with the myosin heads attached to this filament were calculated using the sphere models of the actin monomers and myosin heads according to the formula (Vainstein, 1963)

$$F_{kl}(R, \Psi) = \sum_n G^k_{nl}(R)\exp(-in\Psi), \qquad (A1)$$

where the Fourier-Bessel structural factor G^k_{nl} is:

$$G^k_{nl}(R) = \sum_j f_j(R)J_n(2\pi R r_j)\exp(i[n(\pi/2 - \psi_j) + 2\pi z_j l/c]), \qquad (A2)$$

where $f_j(R)$ is the structural factor of jth sphere; r_j, ψ_j, z_j are polar coordinates of jth sphere; J_n is the nth-order Bessel function of the first kind; R, Ψ are the radial and azimuthal coordinates in reciprocal space; and $c = 214.5$ nm is the axial size of the unit cell.

The intensity of the layer lines was then calculated as the azimuthally averaged square of the Fourier transform, taking into account axial and radial disorder of the thin filaments in the unit cell and disorder in the translation of the unit cells in the super-lattice (Vainstein, 1963).

$$I_l = (1 - \exp(-2M)) \sum_{i=1}^{6} |F_{il}|^2 + \exp(-2M) \sum_{n,m,k,p} G^k_{nl}(G^p_{ml})^*\exp(-2M)C_{n-m} \qquad (A3)$$

where M is the "thermal" factor describing the disorder of the first kind:

$$M = 2\pi^2(R^2\Delta r_A^2 + (l/c)^2\Delta z_A^2); \qquad (A4)$$

Δr_A, Δz_A are the transversal and axial r.m.s. deviations of the actin filaments from their trigonal positions in a unit cell (Fig. 4); $(G^p_{ml})^*$ is the complex conjugate of G^p_{ml}; C_q are coefficients of the Fourier series representing interference function $Z(R, \Psi, l)$ describing the disorder of the second kind of the hexagonal lattice:

$$Z(R, \Psi, l) = 1 + \sum_{s=1}^{3} \frac{2F(\cos\chi_s - F)}{d_s} + \sum_{s=1}^{2} \frac{2F^2(\cos(\chi_s + \chi_{s+1}) - F(\cos\chi_s + \cos\chi_{s+1}) + F^2)}{d_s d_{s+1}} + \frac{2F^2(\cos(\chi_3 - \chi_1) - F(\cos\chi_3 + \cos\chi_1) + F^2)}{d_3 d_1}. \qquad (A5)$$

Here

$$F = \exp(-2\pi^2(R^2\Delta r_T^2 + (l/c)^2\Delta z_T^2)), \qquad (A6)$$

$$\chi_s = 2\pi R\sqrt{3}a\cos\left(\frac{\pi}{6} - (s-1)\frac{\pi}{3} - \Psi\right), \qquad (A7)$$

$$d_s = 1 - 2F\cos\chi_s + F^2, \qquad (A8)$$

$a = 45.5$ nm is the distance between the centers of the neighboring myosin filaments; Δr_T, Δz_T are the transversal and axial r.m.s. deviations of the central myosin filament of a neighbor unit cell from its ideal position in the super-lattice (Fig. 4).

APPENDIX B

Intensity diffracted by a partially occupied helix

We consider diffraction by a structure formed by identical molecules (i.e., myosin heads) bound to some, but not all, points of a discrete helix with u_t symmetry (i.e., there are u helical points in t turns) with the axial distance d between the adjacent points. The binding pattern can be described by the one-dimensional distribution function

$$A(z) = \sum_{j=1}^{U} \rho_j\delta(z - jd) \qquad (B1)$$

where $\rho_s = 1$ if the sth actin binding site is occupied by bound myosin heads and $\rho_s = 0$ if it is left unoccupied; δ is Dirac delta function. We assume that $A(z)$ has a period c which is a multiple of ud: $c = dU$, where $U = ru$ and r is an integer, so that $\rho_s = \rho_{s+U}$. For the model of the actin-myosin lattice used here, $u = 13$, $t = 7$, $U = 78$, $T = rt = 42$, and $d = 2.75$ nm. The cylindrically averaged intensity I_l diffracted by such structure on the lth layer line is given by (Tsaturyan, 2002):

$$I_l(R) = \sum_n \sum_s |G_{nl}(R)|^2 b_s, \qquad (B2)$$

where the Fourier-Bessel structure factors $G_{nl}(R)$ of a single repetitive group of atoms are (Vainstein, 1963)

$$G_{nl}(R) = \sum_{j=1}^{M} f_j J_n(2\pi R r_j)\exp\{i[n(\pi/2 - \varphi_j) + 2\pi l z_j/c]\}, \qquad (B3)$$

f_j is the scattering factor of the jth atom of a bound molecule, r_j, φ_j, and z_j are cylindrical coordinates of this atom, J_n is the nth-order Bessel function

of the first kind, R is the radial coordinate in reciprocal space, and b_s are defined by the expression

$$b_s = \sum_{k,p=0}^{U-1} \rho_k \rho_p \exp[2\pi i(k-p)s/U]. \quad \text{(B4)}$$

In Eq. B2, integer l, n, and s satisfy the selection rule

$$l = nT + mU + s, \quad \text{(B5)}$$

where m also is an integer. This selection rule was originally obtained by Holmes et al. (1980).

As seen from Eq. B2, the symmetrically averaged intensity of a layer line is determined by the Fourier-Bessel structural factors G_{nl} of a single repetitive group of atoms, and by parameters b_s (Eq. B4), which define the one-dimensional interference function

$$B(Z) = \sum_s b_s \delta(Z - s/Ud), \quad \text{(B6)}$$

where Z is the axial coordinate in reciprocal space. $B(Z)$ is the square of the amplitude of the Fourier transform of the one-dimensional distribution function defined by Eq. B1, or in other words the intensity diffracted by a one-dimensional array of point diffractors with unitary scattering power distributed according to Eq. B1.

According to Eq. B2, each non-zero term b_s produces meridional (i.e., proportional to J_0) intensity on the sth layer line. Also, the b_s term contributes to a layer line with index l according to Eq. B5. For myosin heads, only G_{nl} with $-2 \le n \le 2$ are large enough to provide significant contributions to I_l. For example, b_{30} ($=b_{-30}$) contributes to the meridional intensity on the A5 layer line (=M6, $l = 30$, $n = 0$, $m = 0$) and to the off-meridional intensity on the A1 layer line ($l = 6$, $n = -1$, $m = 1$). Besides A1, b_{30} also contributes to the A6 ($l = 36$, $n = 2$, $m = -1$) and A7 (A7, $l = -42$, $n = 2$, $m = -2$) actin layer lines proportionally to the second-order Bessel function, J_2, in addition to their main terms, which are proportional to J_1 and b_0.

Term b_{15} contributes to the meridional reflection on the M3 layer line ($l = 15$, $n = 0$, $m = 0$) and to the off-meridional intensities on the beating actin-myosin layer lines AM_{-1}, AM_{+1} with indices $l = 9$ and $l = 21$, respectively. The contribution of b_{15} (and b_{-15}) to the ninth layer line is proportional to the second-order Bessel function J_2 ($n = -2$, $m = 1$), while its contribution to the 21st layer line comes from both first- and second-order Bessel functions ($n = -1$, $m = 1$ and $n = 2$, $m = -1$).

We are grateful to Prof. Kenneth C. Holmes and his colleagues for open access to the coordinates of the actin-S1 complex before publication, and to Prof. Michael A. Ferenczi for comments on the manuscript.

This work was supported by grants from the Howard Hughes Medical Institute, INTAS, and the Russian Foundation for Basic Research.

REFERENCES

Bershitsky, S. Y., A. K. Tsaturyan, O. N. Bershitskaya, G. I. Machanov, P. Brown, R. Burns, and M. A. Ferenczi. 1997. Muscle force is generated by myosin heads stereospecifically attached to actin. *Nature.* 388: 186–190.

Bershitsky, S. Y., A. K. Tsaturyan, O. Bershitskaya, G. Mashanov, P. Brown, M. Webb, and M. A. Ferenczi. 1996. Mechanical and structural properties underlying contraction of skeletal muscle fibers after partial 1-ethyl-3-[3-(dimethylamino)propyl]carbodiimide cross-linking. *Biophys. J.* 71:1462–1474.

Bordas, J., G. P. Diakun, F. G. Diaz, J. E. Harries, R. A. Lewis, J. Lowy, G. R. Mant, M. L. Martin-Fernandez, and E. Towns-Andrews. 1993. Two-dimensional time-resolved x-ray diffraction studies of live isometrically contracting frog sartorius muscle. *J. Muscle Res. Cell Motil.* 14:311–324.

Brenner, B., S. Xu, J. M. Chalovich, and L. C. Yu. 1996. Radial equilibrium length of actomyosin cross-bridges in muscle. *Biophys. J.* 71: 2751–2758.

Cochran, W., F. H. C. Crick, and V. Vand. 1952. The structure of the synthetic polypeptides. I. The transform of atoms on a helix. *Acta Crystallogr.* 5:581–586.

Cooke, R., M. S. Crowder, and C. H. Wendt. 1984. Muscle cross-bridges. Do they rotate? *In* Contracting Mechanism in Muscle. G. H. Pollack and H. Sugi, editors. Plenum Press, NY, London. 413–423.

Cooke, R., and K. Franks. 1980. All myosin heads bond actin in rigor rabbit skeletal muscle. *Biochemistry.* 19:2265–2269.

Dobbie, I., M. Linari, G. Piazzesi, M. Reconditi, N. Koubassova, M. A. Ferenczi, V. Lombardi, and M. Irving. 1998. Elastic bending and active tilting of myosin heads during muscle contraction. *Nature.* 396:383–387.

Dominguez, R., Y. Freyzon, K. M. Trybus, and C. Cohen. 1998. Crystal structure of a vertebrate smooth muscle myosin motor domain and its complex with the essential light chain: visualization of the pre-power stroke. *Cell.* 94:559–571.

Harford, J., and J. Squire. 1997. Time-resolved diffraction studies of muscle using synchrotron radiation. *Rep. Prog. Phys.* 60:1723–1787.

Haselgrove, J. C., and M. K. Reedy. 1978. Modeling rigor cross-bridge patterns in muscle. I. Initial studies of the rigor lattice of insect flight muscle. *Biophys. J.* 24:713–728.

Holmes, K. C. 1997. The swinging lever arm hypothesis of muscle contraction. *Curr. Biol.* 7:112–118.

Holmes, K. C., J. Kull, W. Jahn, I. Angert, and R. Schröder. 2002. High resolution cryoelectronmicroscopy of decorated actin shows that the actin binding cleft is shut. *J. Gen. Physiol.* In press.

Holmes, K. C., D. Popp, W. Gebhard, and W. Kabsch. 1990. Atomic model of the actin filament. *Nature.* 347:44–49.

Holmes, K. C., R. T. Tregear, and J. Barrington Leigh. 1980. Interpretation of the low angle x-ray diffraction from insect flight muscle in rigor. *Proc. R. Soc. B.* 207:13–33.

Hudson, L., J. J. Harford, R. C. Denny, and J. M. Squire. 1997. Myosin head configuration in relaxed fish muscle: resting state myosin heads must swing axially by up to 150 Å or turn upside down to reach rigor. *J. Mol. Biol.* 273:440–455.

Huxley, H. E. 1996. A personal view of muscle and motility mechanisms. *Annu. Rev. Physiol.* 58:1–19.

Huxley, H. E., and W. Brown. 1967. The low-angle x-ray diffraction of vertebrate striated muscle and its behaviour during contraction and rigor. *J. Mol. Biol.* 30:383–434.

Huxley, H. E., A. R. Faruqi, M. Kress, J. Bordas, and M. H. Koch. 1982. Time-resolved x-ray diffraction studies of the myosin layer-line reflections during muscle contraction. *J. Mol. Biol.* 158:637–684.

Huxley, H. E., A. Stewart, H. Sosa, and T. Irving. 1994. X-ray diffraction measurements of the extensibility of actin and myosin filaments in contracting muscle. *Biophys. J.* 67:2411–2421.

Juanhuix, J., J. Bordas, J. Campmany, A. Svensson, M. L. Bassford, and T. Narayanan. 2001. Axial disposition of myosin heads in isometrically contracting muscles. *Biophys. J.* 80:1429–1441.

Koubassova, N., and A. K. Tsaturyan. 1999. Modelling of cross-bridge binding to actin in skeletal muscle and calculated x-ray diffraction pattern. *J. Muscle Res. Cell Motil.* 20:822–823.

Kraft, T., T. Mattei, and B. Brenner. 1998. Structural features of force-generating cross-bridges. *Adv. Exp. Med. Biol.* 453:289–296.

Kress, M., H. E. Huxley, A. R. Faruqi, and G. Hendrix. 1986. Structural changes during activation of frog muscle studied by time-resolved x-ray diffraction. *J. Mol. Biol.* 188:325–342.

Lewis, R. A., W. I. Helsby, A. O. Jones, C. J. Hall, B. Parker, J. Sheldon, P. Clifford, M. Hillen, I. Sumner, N. S. Fore, R. W. M. Jones, and K. M. Roberts. 1997. The "RAPID" high rate large area x-ray detector system. *Nucl. Instrum. Meth.* A392:32–41.

Linari, M., I. Dobbie, M. Reconditi, N. Koubassova, M. Irving, G. Piazzesi, and V. Lombardi. 1998. The stiffness of skeletal muscle in isometric

contraction and rigor: the fraction of myosin heads bound to actin. *Biophys. J.* 74:2459–2473.

Linari, M., G. Piazzesi, I. Dobbie, N. Koubassova, M. Reconditi, T. Narayanan, O. Diat, M. Irving, and V. Lombardi. 2000. Interference fine structure and sarcomere length dependence of the axial x-ray pattern from active single muscle fibers. *Proc. Natl. Acad. Sci. USA.* 97: 7226–7231.

Lorenz, M., D. Popp, and K. C. Holmes. 1993. Refinement of the F-actin model against x-ray fiber diffraction data by the use of a directed mutation algorithm. *J. Mol. Biol.* 234:826–836.

Lovell, S. J., P. J. Knight, and W. F. Harrington. 1981. Fraction of myosin heads bound to thin filaments in rigor fibrils from insect flight and vertebral muscle. *Nature.* 293:664–666.

Luther, P. K., and J. M. Squire. 1980. Three-dimensional structure of the vertebrate muscle A-band. II. The myosin filament superlattice. *J. Mol. Biol.* 141:409–439.

Malinchik, S. B., and V. V. Lednev. 1992. Interpretation of the x-ray diffraction pattern from relaxed skeletal muscle and modelling of the thick filament structure. *J. Muscle Res. Cell Motil.* 13:406–419.

Malinchik, S., S. Xu, and L. C. Yu. 1997. Temperature-induced structural changes in the myosin thick filament of skinned rabbit psoas muscle. *Biophys. J.* 73:2304–2312.

McLaughlin, R. J. 1977. Systematic design of cantilever beams for muscle research. *J. Appl. Physiol.* 42:786–794.

Mendelson, R., and E. P. Morris. 1997. The structure of the acto-myosin subfragment 1 complex: results of searches using data from electron microscopy and x-ray crystallography. *Proc. Natl. Acad. Sci. USA.* 94:8533–8538.

Rayment, I., H. M. Holden, M. Whittaker, C. B. Yohn, M. Lorenz, K. C. Holmes, and R. A. Milligan. 1993a. Structure of the actin-myosin complex and its implications for muscle contraction. *Science.* 261: 50–58.

Rayment, I., W. R. Rypniewski, K. Schmidt-Bäse, R. Smith, D. R. Tomchick, M. M. Benning, D. A. Winkelmann, G. Wesenberg, and H. M. Holden. 1993b. Three dimensional structure of subfragment-1: a molecular motor. *Science.* 261:58–65.

Squire, J. M., and J. J. Harford. 1988. Actin filament organization and myosin head labeling patterns in vertebrate skeletal muscles in the rigor and weak binding states. *J. Muscle Res. Cell Motil.* 9:344–358.

Stewart, M., A. D. McLachlan, and C. R. Calladine. 1987. A model to account for the elastic element in muscle crossbridges in terms of a bending myosin rod. *Proc. R. Soc. Lond. B.* 229:381–413.

Takezawa, Y., D. S. Kim, M. Ogino, Y. Sugimoto, T. Kobayashi, T. Arata, and K. Wakabayashi. 1999. Backward movements of cross-bridges by application of stretch and by binding of MgADP to skeletal muscle fibers in the rigor state as studied by x-ray diffraction. *Biophys. J.* 76:1770–1783.

Thirlwell, H., J. R. T. Corrie, G. P. Reid, D. R. Trentham, and M. A. Ferenczi. 1994. Kinetics of relaxation from rigor of permeabilized fast-twitch fibers from the rabbit using a novel caged-ATP and apyrase. *Biophys. J.* 67:2436–2447.

Tsaturyan, A. K. 2002. Diffraction on partially decorated helices. *Acta Crystallogr. A.* A58:292–294.

Vainstein, B. K. 1963. Diffraction of X-rays by chain molecules. Izdatelstvo Akademii Nauk SSSR, Moscow.

Varriano-Marston, E., C. Franzini-Armstrong, and J. C. Haselgrove. 1984. The structure and disposition of cross-bridges in deep-etched fish muscle. *J. Muscle Res. Cell Motil.* 5:363–386.

Wakabayashi, K., Y. Sugimoto, H. Tanaka, Y. Ueno, Y. Takezawa, and Y. Amemiya. 1994. X-ray diffraction measurements for the extensibility of actin and myosin filaments during muscle contraction. *Biophys. J.* 67: 2422–2435.

Xu, S., S. Malinchik, D. Gilroy, Th. Kraft, B. Brenner, and L. C. Yu. 1997. X-ray diffraction studies of cross-bridges weakly bound to actin in relaxed skinned fibers of rabbit psoas muscle. *Biophys. J.* 73:2292–2303.

Yagi, N. 1991. Intensification of the first actin layer-line during contraction of frog skeletal muscle. *Adv. Biophys.* 27:35–43.

Yagi, N. 1996. Labelling of thin filaments by myosin heads in contracting and rigor vertebrate skeletal muscles. *Acta Crystallogr D.* 52: 1169–1173.